Transactions of Tianjin University (2021) 27:348–357
https://doi.org/10.1007/s12209-021-00291-x

RESEARCH ARTICLE

Simultaneously Efficient Solar Light Harvesting and Charge Transfer of Hollow Octahedral Cu_2S/CdS p–n Heterostructures for Remarkable Photocatalytic Hydrogen Generation

Yanting Zhang[1] · Lei Ran[1] · Zhuwei Li[1] · Panlong Zhai[1] · Bo Zhang[1] · Zhaozhong Fan[1] · Chen Wang[1] · Xiaomeng Zhang[1] · Jungang Hou[1] · Licheng Sun[2,3]

Received: 24 March 2021 / Revised: 29 March 2021 / Accepted: 30 March 2021 / Published online: 21 May 2021

Abstract

Solar-driven water splitting is a promising alternative to industrial hydrogen production. This study reports an elaborate design and synthesis of the integration of cadmium sulfide (CdS) quantum dots and cuprous sulfide (Cu_2S) nanosheets as three-dimensional (3D) hollow octahedral Cu_2S/CdS p–n heterostructured architectures by a versatile template and one-pot sulfidation strategy. 3D hierarchical hollow nanostructures can strengthen multiple reflections of solar light and provide a large specific surface area and abundant reaction sites for photocatalytic water splitting. Owing to the construction of the p–n heterostructure as an ideal catalytic model with highly matched band alignment at Cu_2S/CdS interfaces, the emerging internal electric field can facilitate the space separation and transfer of photoexcited charges between CdS and Cu_2S and also enhance charge dynamics and prolong charge lifetimes. Notably, the unique hollow Cu_2S/CdS architectures deliver a largely enhanced visible-light-driven hydrogen generation rate of 4.76 mmol/(g·h), which is nearly 8.5 and 476 times larger than that of pristine CdS and Cu_2S catalysts, respectively. This work not only paves the way for the rational design and fabrication of hollow photocatalysts but also clarifies the crucial role of unique heterostructure in photocatalysis for solar energy conversion.

Keywords Hollow octahedrons · P–n heterostructure · Charge separation · Photocatalytic water splitting

Introduction

Since the increasingly serious global environmental pollution and energy crisis greatly influence the sustainable development of society, it is urgent to explore clean and renewable solar energy conversion systems [1]. Photocatalytic water splitting has attracted tremendous attention as a catholicon to the worldwide energy dilemma, converting solar energy resources into clean oxygen and hydrogen fuels [2]. To date, a large number of semiconductors such as metal oxides, chalcogenides, nitrides, and oxynitrides have been widely employed as photocatalytic materials [3]. Specifically, metal chalcogenides exhibit great potential in the field of solar energy conversion [4]. Among these semiconductor materials, due to various merits such as narrow bandgap and suitable band energy position, the n-type CdS is regarded as a prominent sulfide for solar energy conversion, particularly in solar hydrogen generation [3]. Meanwhile, the p-type copper sulfide is a good catalyst due to its relatively narrow bandgap and suitable band edge positions [3, 4]. However, a series of dilemmas lie in single metal sulfide-based photocatalysts, such as limited light harvesting, poor charge-carrier mobility, high bulk recombination, and large surface kinetic barrier for water-splitting reaction, resulting in unsatisfactory photoconversion efficiency and poor photocatalytic stability.

It is well known that nanostructure engineering has been regarded as a promising approach to regulate the

Yanting Zhang and Lei Ran contributed equally to this work.

✉ Jungang Hou
jhou@dlut.edu.cn

✉ Licheng Sun
lichengs@kth.se

[1] State Key Laboratory of Fine Chemicals, School of Chemical Engineering, Dalian University of Technology, Dalian 116024, China

[2] Center of Artificial Photosynthesis for Solar Fuels, School of Science, Westlake University, Hangzhou 310024, China

[3] Department of Chemistry, School of Engineering Sciences in Chemistry, Biotechnology and Health, KTH Royal Institute of Technology, 10044 Stockholm, Sweden

light-harvesting capacity and endow active sites to optimize the charge separation and transfer, thus promoting photocatalytic performance [5–7]. Among various nanostructures, three-dimensional (3D) hierarchical materials received extensive attention owing to their unique physical and chemical advantages. Particularly, hollow architectures with a larger surface area and abundant reactive sites can enhance solar light utilization and photocatalytic performance [8–14]. For example, hierarchical Co_9S_8@$ZnIn_2S_4$ heterostructures as photocatalysts exhibited an excellent hydrogen production rate of 6250 μmol/(g·h) for photocatalytic water splitting [12]. Hierarchical Co/NGC@$ZnIn_2S_4$ hollow heterostructures without cocatalyst presented superior hydrogen generation activity and outstanding stability [13]. Hollow La/Rh-doped $SrTiO_3$ nanostructures showed a highly efficient hydrogen generation rate owing to their high light absorption ability [14]. Thus, it is a challenge to develop hollow metal chalcogenides nanostructures for photocatalytic water splitting.

Owing to the sluggish charge-carrier separation in various semiconductors, the photocatalytic performance is still far below what is expected. Aiming at these issues, diverse approaches have been exploited to address, such as heteroatoms doping [15], dye sensitization [16], defect engineering [17, 18], and heterostructure engineering [19, 20]. Among these strategies, heterojunction engineering has been considered an effective tool to suppress the photoexcited charge recombination and optimize photocatalytic performance. For instance, Co_9S_8/CdS hollow nanocube photocatalyst showed enhanced light capture and photocatalytic activity compared to solid Co_9S_8/CdS nanocubes [21]. NiS/$Zn_xCd_{1-x}S$ heterojunctions were synthesized by the direct conversion of the metal–organic framework, yielding a high photocatalytic hydrogen generation rate and high stability under visible-light irradiation [22]. Co_9S_8/Cd/CdS tubular heterostructures exhibited a photocatalytic hydrogen generation rate of up to 10.42 μmol/h due to the Z-scheme transition metal bridge [23]. Porous CuS/ZnS nanosheet photocatalysts prepared by hydrothermal and cation exchange reaction showed a high photocatalytic hydrogen generation rate of 4147 μmol/(g·h) based on the photoinduced interfacial charge transfer process [24]. Inspired by nanostructure engineering and heterostructure engineering, it is important to construct hollow heterostructures of metal chalcogenides for enhanced photocatalytic hydrogen production.

This work reports an elaborate design and synthesis of the integration of CdS quantum dots (QDs) and Cu_2S nanosheets (NSs) as 3D hollow octahedral Cu_2S/CdS p–n heterostructured architectures by a versatile template and one-pot sulfidation strategy. Compared to the pristine hollow Cu_2S and CdS photocatalysts, as-synthesized hollow octahedral Cu_2S/CdS p–n heterostructures exhibited an impressively high photocatalytic hydrogen generation rate of 4.76 mmol/(g·h) and excellent stability under solar energy irradiation, which was over 8.5 and 476 times higher than that of pure CdS and hollow Cu_2S octahedrons photocatalysts, respectively. Notably, the enhanced photocatalytic hydrogen generation performance of hollow octahedral Cu_2S/CdS p–n heterostructures is ascribed to the strong light-harvesting capacity, efficient charge transfer and separation, and abundant active sites through the construction of hollow architectures.

Experimental

Fabrication of Cu_2S/CdS Heterostructures

Cu_2O octahedrons were synthesized by a modified approach from a previous report [25]. A certain amount of Cu_2O octahedrons was uniformly dispersed in 20 mL of deionized (DI) water under ultrasonic treatment for 10 min. $Cd(CH_3COO)_2{\cdot}2H_2O$ was then added to the above solution under magnetic stirring for 20 min. Then, 10 mL of Na_2S aqueous solution (0.01 M) was added to the uniform precursor solution at room temperature. The products were obtained by centrifugation, washed three times, and dried in a vacuum condition. Thus, a sequence of Cu_2S/CdS-*X* with $X = 0$, 5wt%, 10wt%, and 20wt% were named as Cu_2S, Cu_2S/CdS-5, Cu_2S/CdS-10, and Cu_2S/CdS-20, respectively. In comparison, CdS nanoparticles were obtained by a similar synthesis process except for the absence of a Cu_2O precursor.

Instruments and Photocatalysts Characterization

Powder X-ray diffraction (XRD) patterns were obtained by an X-ray diffractometer equipped with graphite monochromatized high-intensity Cu Kα radiation ($\lambda = 1.54178$ Å). SEM images were captured by a field-emission scanning electron microscope (FESEM, FEI Nova Nano SEM 450). TEM images were performed on a transmission electron microscope (TEM, FEI TF30) and a high-resolution TEM (HRTEM). The N_2 adsorption–desorption curves were obtained by the Micromeritics ASAP 2460 surface areas and porosities profiler. Specific surface areas were acquired via the Brunauer–Emmett–Teller (BET) approach, and X-ray photoelectron spectroscopy (XPS, ESCALAB 250) was employed to explore the elemental composition and valence states of materials. Finally, UV–Vis absorption and photoluminescence (PL) spectra were measured by a UV–Vis–NIR spectrophotometer (Shimadzu UV-3600 Plus) and a fluorescence spectrometer (Horiba, FloroMax-4P).

Photocatalytic Tests

Photocatalytic hydrogen generation tests were performed using visible-light illumination. The reaction vessel used in

this study was a unilateral irradiation Pyrex container linked to a sealed gas circulator and exhaust system under room temperature, in which a xenon light source (300 W) was placed ~ 25 cm away from the system. For a regular photocatalytic water-splitting test, a certain amount (5 mg) of different photocatalysts and lactic acid (LA, 1 mL) as the hole scavenger were dispersed in 9 mL DI water. Before illumination, the reaction cell was ensured under anaerobic conditions without oxygen by a degassing process. In the photocatalytic process, the reactant system steadily proceeded under visible-light irradiation ($\lambda > 400$ nm) and ambient temperature by a circulating water system. To assess the photocatalytic stability of the photocatalyst in a long-term operation, the recycled photocatalytic hydrogen production measurements were performed under the same condition. The apparent quantum efficiency (AQE) can be determined via the same photocatalytic test procedure under visible-light irradiation. The generated hydrogen production amount was analyzed via a gas chromatograph (GC2014).

Results and Discussion

Synthesis and Characterization

Figure 1a presents the elaborate design and synthesis of the hollow octahedral Cu_2S/CdS p–n heterostructure as an ideal catalytic model. First, Cu_2O octahedrons were produced as a template. Second, hollow octahedral Cu_2S/CdS heterostructures assembled by Cu_2S nanosheets and CdS quantum dots were fabricated by this versatile sulfidation synthesis strategy. FESEM and TEM were employed to explore the morphology and structure evolution of as-prepared Cu_2S/CdS heterostructure. As shown in Fig. 1b, Cu_2O nano-octahedrons exhibit an average size of ~ 400 nm. SEM images of Cu_2S and Cu_2S/CdS present the nanosheet-assembled architectures (Fig. 1c and d). To confirm, EDS mappings were obtained as shown in Fig. 1e–g and Fig. S1, which indicate the existence of elements Cu, Cd, and S, demonstrating the homogeneous distribution in Cu_2S and Cu_2S/CdS octahedrons. In comparison, the morphology and average size of Cu_2S/CdS octahedrons are similar to those of Cu_2S (Figs. S1 and S2), exhibiting a hierarchical morphology and a size of ~ 500 nm for Cu_2S and Cu_2S/CdS octahedrons.

TEM images of Cu_2S/CdS hybrid in Fig. 2a and b reveal an octahedral and hollow nanostructure with a homogeneous size of 500 nm, indicating that the one-pot sulfidation treatment can convert the solid into nano-octahedrons with ultrathin nanosheet-assembled hierarchical morphology (Fig. 2c). Dispersed Cu_2S hollow octahedrons were also evident in the TEM image (Fig. S2). As shown in the HRTEM image in Fig. 2d, the lattice fringe of 0.34 nm corresponds well to the (111) plane of a cubic CdS phase, revealing the favorable crystallinity of CdS [26], while the interplanar spacing of 0.189 nm is ascribed to the (573) facet of a tetragonal Cu_2S [27]. The selected-area electron diffraction pattern in Fig. 2e shows that the diffraction rings correspond well with the (573) plane of Cu_2S and the (220) plane of CdS, demonstrating the successful preparation of the Cu_2S/CdS binary composite. The corresponding elemental mapping images obtained via high-angle annular dark-field scanning transmission electron microscopy (HAADF-STEM) for Cu_2S/CdS present a uniform distribution of Cu, Cd, and S species (Fig. 2f–i). Thus, SEM and TEM images indicate that the hollow Cu_2S/CdS octahedron heterostructures can be synthesized by this versatile strategy.

Furthermore, XRD patterns were employed to verify the phase composition of the products. The observed diffraction peaks in Fig. 3a belong to the reflections of tetragonal Cu_2S (JCPDF 02–1294), while the other diffraction peaks are indexed to the reflections of cubic CdS (JCPDS 10–0454), confirming the synthesis of Cu_2S/CdS composites. XPS was also performed to check the elemental compositions and valence states. In the full range survey spectrum of Cu_2S/CdS (Fig. 3b), the peaks of Cu 2p, Cd 3d, and S 2p can be examined. The two binding energies that are centered at 932.3 eV and 952.2 eV in the Cu 2p XPS spectrum (Fig. 3c) can be ascribed to Cu $2p_{3/2}$ and Cu $2p_{1/2}$, respectively, confirming the presence of Cu^+ in Cu_2S [28]. However, the Cd 3d XPS spectrum (Fig. 3d) reveals two obvious peaks at 405.0 and 411.7 eV, which correspond to Cd $3d_{5/2}$ and Cd $3d_{3/2}$, proving the presence of Cd^{2+} in the binary hybrid [29]. Meanwhile, the peaks at 161.8 and 162.7 eV in the S 2p XPS spectrum (Fig. 3e) are derived from S $2p_{3/2}$ and S $2p_{1/2}$, indicating the existence of the S^{2-} bonding to Cd^{2+} and Cu^+ [30]. Similarly, Cu^+ and S^{2-} species can also be detected in Cu_2S from the analysis of Cu 2p and S 2p XPS spectra in Fig. S3. Moreover, nitrogen adsorption–desorption tests were applied. As shown in Fig. 3f, all products display analogical shape plots, in which characteristic type IV curves with H3 hysteresis loops ($P/P_0 > 0.4$) are obviously detected by the Brunauer–Emmett–Teller (BET) surface area analysis, proving the mesopore feature of the products. The Barrett–Joyner–Halenda (BJH) analysis of the pore size distribution plots (Fig. S4) presents the specific surface area, pore size, and pore volume. Cu_2S/CdS exhibits the largest specific surface area (129.7 m^2/g) among all products, thereby affording superior photocatalytic activity due to abundant active sites [31]. The larger pore size of Cu_2S/CdS than that of Cu_2S may have resulted from the filling of CdS QDs into the mesoporous Cu_2S/CdS heterostructures.

To illustrate the vital function of the hollow nanostructure for solar energy capture, UV–Vis absorption spectra were recorded to explore the light response features of the products. As shown in Fig. 5a, a characteristic absorption edge in the visible-light range can be observed at ~ 510 nm

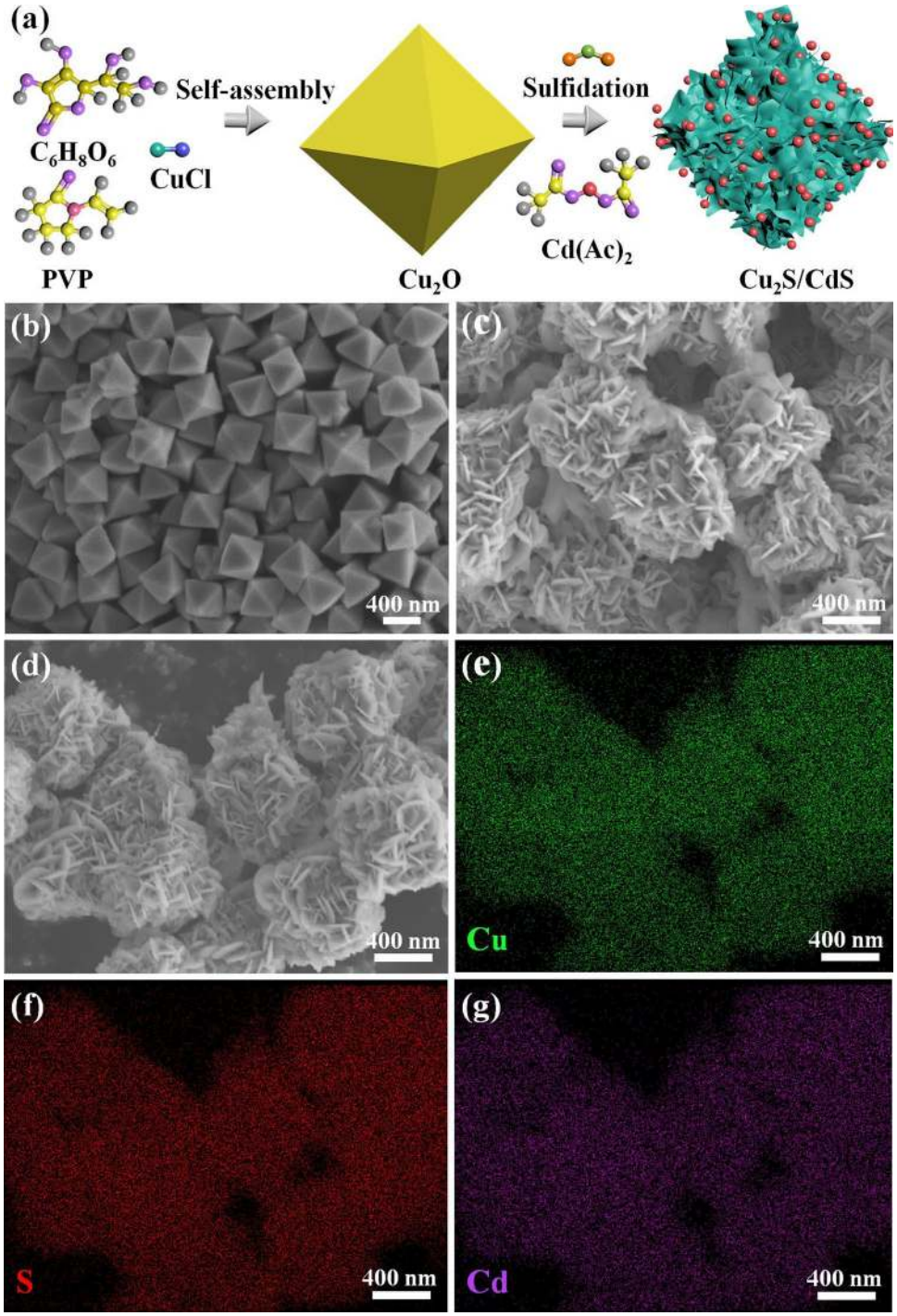

Fig. 1 **a** The synthesis protocol for the construction of hollow Cu_2S/CdS heterostructure. SEM images of **b** Cu_2O, **c** Cu_2S/CdS, and **d** Cu_2S element mappings of Cu_2S/CdS for **e** copper, **f** sulfur, and **g** cadmium

for CdS [32]. Notably, hollow octahedrons exhibit a stronger light absorption than other products due to the multiple reflections of incident light inside the hollow nanostructure [8–14]. The improved light capture derived from the hollow structure is expected to enhance the light response capacity of Cu_2S/CdS for photocatalytic application. Meanwhile, the bandgap energies of the products can be determined using the Tauc's relation based on the absorption edges. As displayed in Fig. S5, the calculated bandgap values of Cu_2S and CdS are 1.1 and 2.4 eV, respectively. Mott–Schottky curves (Fig. S6) were used to explore the band positions of the semiconductors [33], corresponding the bandgap structures of CdS and Cu_2S in Fig. S7. Based on the positions of conduction band (CB) and valence band (VB) for CdS and Cu_2S, the photoexcited electrons and holes can be effectively transferred and separated in Cu_2S/CdS heterostructures. Thus, the construction of Cu_2S/CdS heterostructures is beneficial to the charge

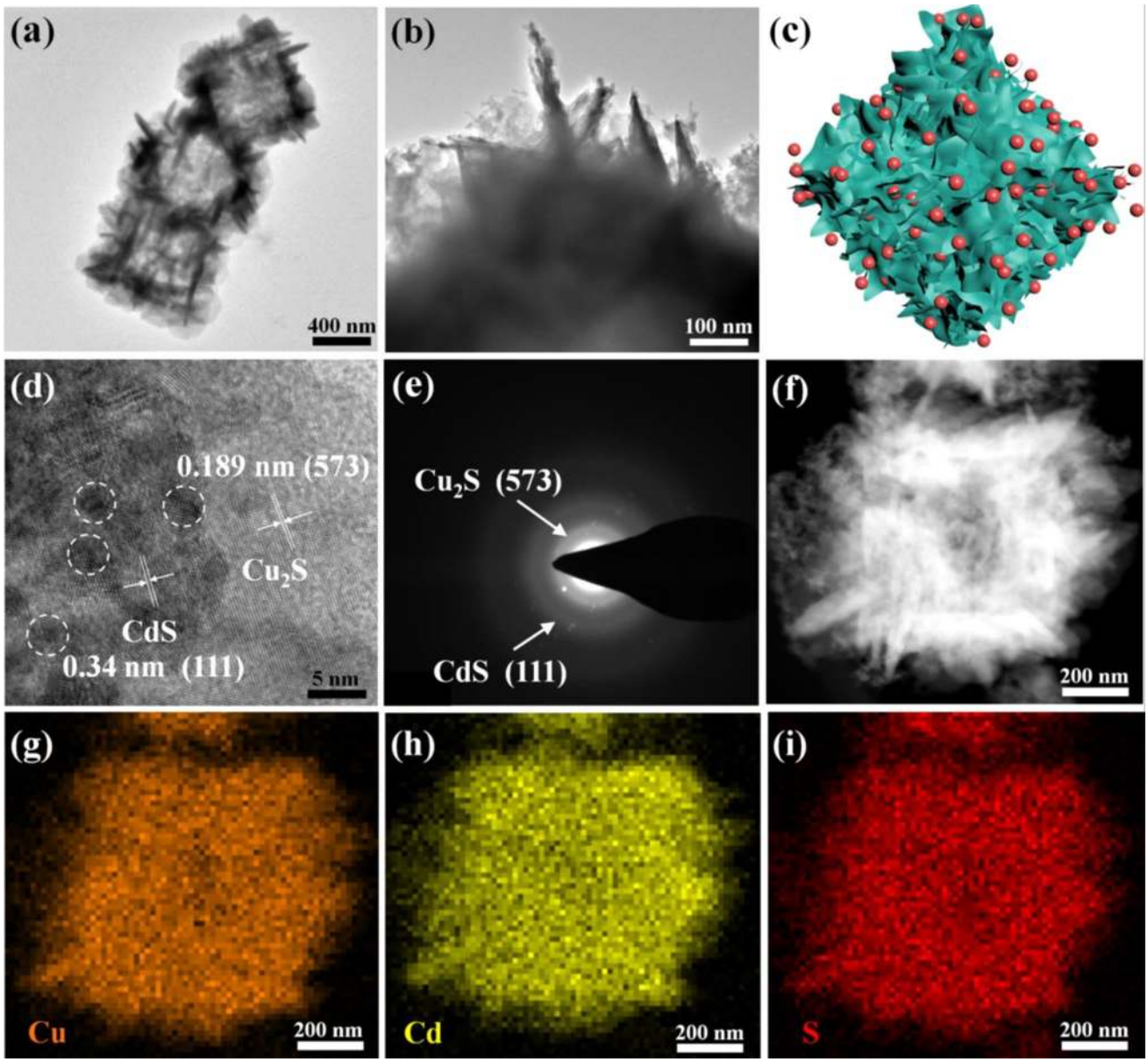

Fig. 2 **a**, **b** TEM images, **c** illustration of the heterostructure, **d** HRTEM image, **e** selected-area electron diffraction pattern, **f** dark-field STEM image and HAADF-STEM element mappings of Cu_2S/CdS for **g** copper, **h** cadmium, and **i** sulfur

transfer and separation, which can consequently enhance the photocatalytic performance.

Photocatalytic Activity and Mechanism Analysis

The photocatalytic hydrogen production of different catalysts was conducted under visible-light irradiation ($\lambda > 400$ nm). As depicted in Fig. 4a, both CdS and Cu_2S catalysts present low H_2 generation rates. However, all Cu_2S/CdS heterostructures exhibit a significantly improved photocatalytic H_2 generation rate by loading various amounts of CdS quantum dots on the surface of Cu_2S nanosheets. With the increasing content of CdS QDs, the photocatalytic H_2 generation rate increases for the as-prepared Cu_2S/CdS heterostructures. However, a decreased H_2 generation rate was observed for the Cu_2S/CdS heterostructures with high content of up to 20 wt% of CdS QDs. In comparison, the obtained hollow and octahedral Cu_2S/CdS-10 photocatalyst exhibits an average hydrogen generation rate of 4.76 mmol/(g·h), which is 8.5 and 476 times larger than that of CdS (0.56 mmol/(g·h)) and Cu_2S (0.01 mmol/(g·h)), respectively. This hydrogen generation rate is higher than those of many photocatalysts such as CdS/Ni-MOF, RP/CoP/$Cd_{0.9}Zn_{0.1}S$, Au/CdS/ZnO, BP/Cu_7S_4, $Cd_{0.5}Zn_{0.5}S$, $BiVO_4$/Au/CdS, CdS/$Ni(OH)_2$,

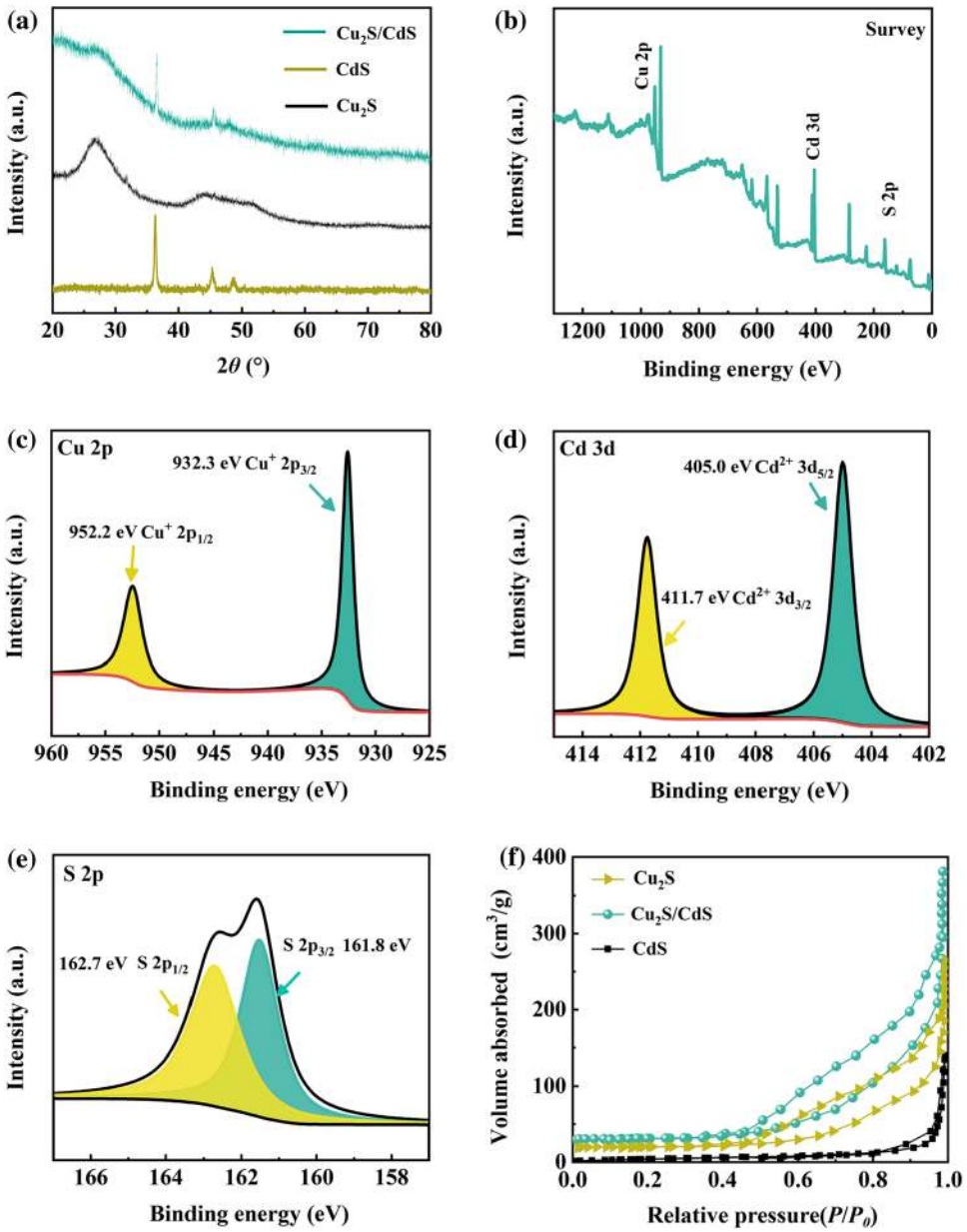

Fig. 3 **a** XRD patterns of Cu_2S, CdS, and Cu_2S/CdS. **b** Survey spectrum, high-resolution XPS spectrum of **c** Cu 2p region, **d** Cd 3d region, and **e** S 2p region for Cu_2S/CdS. **f** N_2 adsorption–desorption isotherms of Cu_2S, CdS, and Cu_2S/CdS

Cu_7S_4/CdS, and Pt-CdS/g-C_3N_4 (Table S1). Moreover, the relationship between photocatalytic activity and illumination time was also probed. As shown in Fig. 4b, all Cu_2S/CdS heterostructures exhibit a linear increasing trend for photocatalytic hydrogen generation during 6-h light illumination.

Since photocatalytic hydrogen generation stability is an essential standard of superior photocatalysts, a stability test was performed for a continuous 30-h illumination. A constant H_2 generation rate of Cu_2S/CdS was observed (Fig. 4c), suggesting its excellent stability. In contrast, the H_2 generation rate for the pristine CdS catalyst (Fig. S8) lowers by 35.6% under the same condition. The corresponding AQE was then calculated. Cu_2S/CdS shows high AQE values of ~ 23.6%, 3.4%, and 1.2% at 420, 450, and 500 nm (Fig. 4d), respectively. Particularly, the original hollow octahedron architecture is still maintained for the Cu_2S/CdS hybrid after long-term photocatalytic reaction as evident in the SEM image (Fig. S9), indicating outstanding stability of Cu_2S/CdS heterostructures.

Photoluminescence spectroscopy (PL) was conducted to verify the charge transfer behavior of the products. As displayed in Fig. 5b, Cu_2S/CdS exhibits the lowest PL intensity compared to the pristine CdS and Cu_2S, indicating that the heterostructure can remarkably suppress the photoexcited

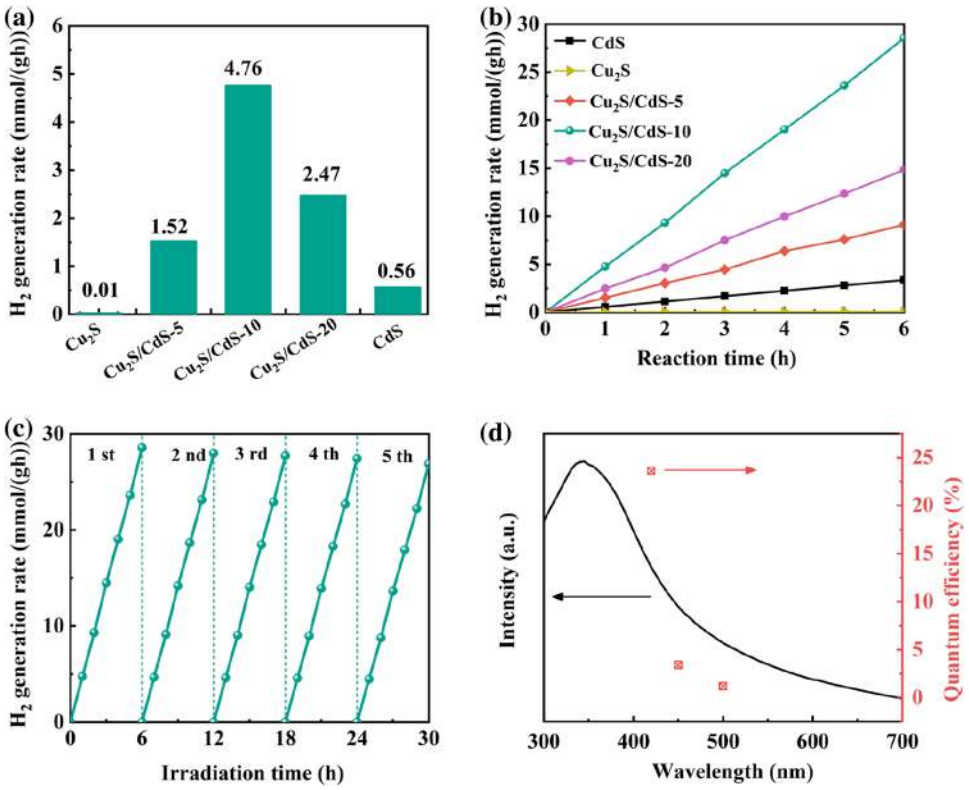

Fig. 4 **a** Apparent hydrogen generation rates and **b** photocatalytic hydrogen generation in 6 h under visible-light irradiation of Cu_2S/CdS with various amounts of CdS. **c** Photocatalytic hydrogen generation stability of Cu_2S/CdS. **d** Wavelength dependence of apparent quantum efficiency and UV–Vis absorption spectra for Cu_2S/CdS

charge recombination, consequently promoting excellent photocatalytic performance [34]. Photoelectrochemical (PEC) water splitting measurements were also performed to study the photoinduced charge generation and separation of Cu_2S, Cu_2S/CdS, and CdS (Fig. S10). As presented in Fig. 5c, the amperometric photocurrent–time curves were conducted under chopped solar irradiation. The Cu_2S/CdS heterostructure exhibits a swift and renewable photocurrent production under switching on/off illumination. Particularly, the Cu_2S/CdS heterostructure photoelectrode exhibits a larger photocurrent density than those of the pristine Cu_2S and CdS. The as-synthesized Cu_2S/CdS photoelectrode displays the largest photocurrent density of 16.9 μA/cm^2, which is larger than those of the pristine Cu_2S and CdS. This indicates that the photoinduced electron–hole pairs can be efficiently separated under solar illumination. Furthermore, electrochemical impedance spectroscopy plots were also recorded to observe the photoinduced charge transfer kinetics on the interface of different photocatalysts [35–42]. Obviously, the small semicircle of the Cu_2S/CdS heterostructure in comparison with the pristine Cu_2S and CdS is observed in Fig. 5d, revealing the small charge transfer resistance and faster interfacial charge transport in Cu_2S/CdS. On account of the above analysis, the introduction of CdS QDs plays an important role in the remarkable photocatalytic hydrogen production activities. Furthermore, the charge transportation efficiencies of CdS and Cu_2S/CdS were quantitatively probed via the time-resolved photoluminescence spectroscopy. From the fitted results in Fig. 5e and f, the Cu_2S/CdS heterostructure exhibits a longer decay time ($\tau = 1.21$ ns) than that of pure CdS ($\tau = 0.055$ ns). The remarkably prolonged lifetime of the Cu_2S/CdS hybrid reveals the accelerated separation of photoinduced electron/hole pairs in the Cu_2S/CdS heterostructure system. Particularly, the electron–hole pairs can be directionally transferred by the internal electric field as the driving force and be accumulated on different semiconductors due to the well-matched band alignment. Thus, charge recombination is effectively restrained, consequently enhancing the charge transfer and separation of Cu_2S/CdS heterostructures.

According to the aforementioned analysis, a possible mechanism for excellent photocatalytic water splitting of Cu_2S/CdS heterostructures can be proposed. First, the hollow nanostructure allows multiple reflections of solar light inside the cavity, generating a large number of electron–hole pairs in the binary composite and, therefore, enhancing photocatalytic water-splitting performance. Moreover, the unique hierarchical nanostructures by the integration of CdS QDs and Cu_2S NSs can provide a larger specific surface area and porous structure, provide more active sites for the

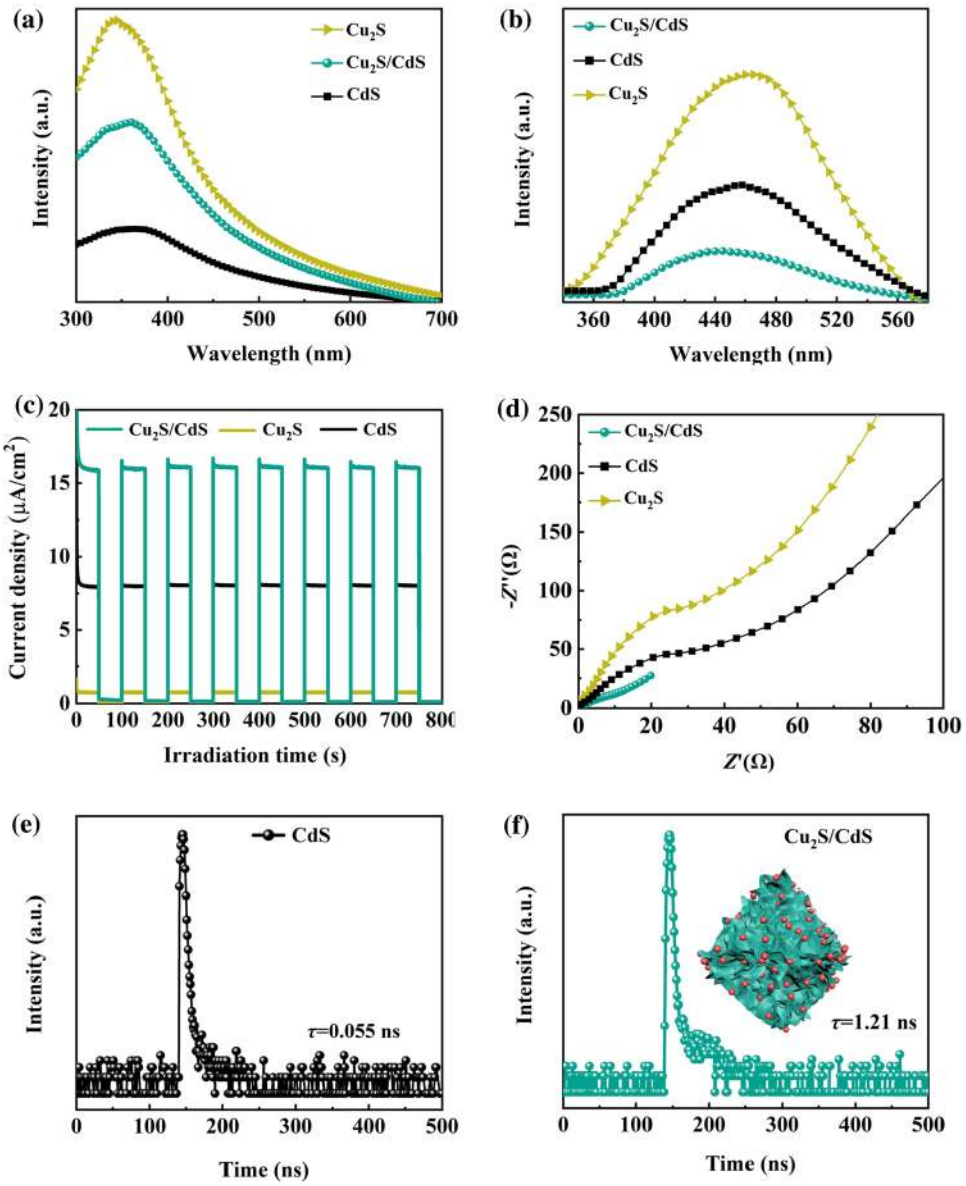

Fig. 5 **a** UV–Vis absorption spectra, **b** photoluminescence spectra, **c** photocurrent responses under chopped light, **d** electrochemical impedance spectra under visible-light irradiation, and **e** time-resolved photoluminescence spectra of CdS and Cu_2S/CdS

photocatalytic reactions, and create a passageway for gas release in the water-splitting system. The heterostructure is then expected at the intimate interface between CdS QDs and Cu_2S NSs on account of the well-matched band edge positions of Cu_2S and CdS. The hollow Cu_2S/CdS heterostructure produced by the template and one-pot sulfidation strategy then results in the efficient transfer of photoexcited charges at the intimate interfaces. Thus, this typical Cu_2S/CdS heterostructure can not only effectively inhibit the photoexcited charge recombination, which consequently accelerates the charge transfer and separation, but also enhance the photocatalytic performance and stability of hollow Cu_2S/CdS heterostructures.

Conclusions

In summary, this work developed an elaborate design and synthesis of the integration of CdS QDs and Cu_2S nanosheets as 3D hollow octahedral Cu_2S/CdS p–n heterostructures by a versatile template and one-pot sulfidation strategy. Notably, the unique hollow Cu_2S/CdS architectures delivered a largely enhanced visible-light-driven hydrogen generation rate of 4.76 mmol/(g·h), which is nearly 8.5 and 476 times larger than that of the pristine CdS and Cu_2S catalysts, respectively. The enhanced photocatalytic hydrogen generation performance of hollow octahedral Cu_2S/CdS p–n heterostructures is ascribed to the strong light-harvesting

capacity, efficient charge transfer and separation, and abundant active sites through the construction of hollow architectures. 3D hierarchical hollow nanostructures can strengthen multiple reflections of solar light and provide a large specific surface area and abundant reaction sites for photocatalytic water splitting. Owing to the construction of the p–n heterostructure as an ideal catalytic model with a highly matched band alignment at the Cu_2S/CdS interfaces, the emerging internal electric field can not only facilitate the space separation and transfer of photoexcited charges between CdS and Cu_2S, but also enhance the charge dynamics and prolong the charges' lifetimes. This work does not only provide an in-depth insight into the rational design and construction of hollow photocatalysts but also clarify the crucial role of unique heterostructures in photocatalysis for energy conversion applications.

Acknowledgements This work was supported by National Natural Science Foundation of China (No. 21972015), Young Top Talents Project of Liaoning Province (No. XLYC1907147), Joint Research Fund Liaoning–Shenyang National Laboratory for Materials Science (No. 2019JH3/30100003), the Fundamental Research Funds for the Central Universities (No. DUT20TD06), the Swedish Research Council, and the K&A Wallenberg Foundation.

References

1. Munir AB, Muhammad-Sukki F, Bani NA (2016) Renewables: solar energy needs focus. Nature 529(7587):466
2. Wu H, Tan HL, Toe CY et al (2020) Photocatalytic and photoelectrochemical systems: similarities and differences. Adv Mater 32(18):e1904717
3. Zhang XM, Liang HC, Li HZ et al (2020) Sequential chemistry toward core-shell structured metal sulfides as stable and highly efficient visible-light photocatalysts. Angewandte Chemie Int Ed 59(8):3287–3293
4. Wang PF, Shen ZR, Xia YG et al (2019) Atomic insights for optimum and excess doping in photocatalysis: a case study of few-layer Cu-$ZnIn_2S_4$. Adv Funct Mater 29(3):1807013
5. Gao HW, Liu C, Jeong HE et al (2012) Plasmon-enhanced photocatalytic activity of iron oxide on gold nanopillars. ACS Nano 6(1):234–240
6. Hou JG, Yang C, Cheng HJ et al (2014) High-performance p-Cu_2O/n-TaON heterojunction nanorod photoanodes passivated with an ultrathin carbon sheath for photoelectrochemical water splitting. Energy Environ Sci 7(11):3758–3768
7. Hou JG, Cheng HJ, Zhu HM et al (2015) Three-dimensional bimetal graphene semiconductor coaxial nanowire arrays to harness charge flow for the photochemical reduction of carbon dioxide. Angew Chem Int Ed 127(29):8600–8604
8. Guo MJ, Zhao TY, Xing ZP et al (2020) Hollow octahedral $Cu_{2-x}S$/CdS/Bi_2S_3 p-n-p type tandem heterojunctions for efficient photothermal effect and robust visible-light-driven photocatalytic performance. ACS Appl Mater Interfaces 12(36):40328–40338
9. Huang Y, Fang YJ, Lu XF et al (2020) Co_3O_4 hollow nanoparticles embedded in mesoporous walls of carbon nanoboxes for efficient lithium storage. Angew Chem Int Ed 59(45):19914–19918
10. Zhang P, Luan DY, Lou XW et al (2020) Fabrication of CdS frame-in-cage particles for efficient photocatalytic hydrogen generation under visible-light irradiation. Adv Mater 32(39):2004561
11. Wang Y, Wang SB, Zhang SL et al (2020) Formation of hierarchical $FeCoS_2$-CoS_2 double-shelled nanotubes with enhanced performance for photocatalytic reduction of CO_2. Angew Chem Int Ed 59(29):11918–11922
12. Wang SB, Guan BY, Lou XWD et al (2018) Construction of $ZnIn_2S_4$-In_2O_3 hierarchical tubular heterostructures for efficient CO_2 photoreduction. J Am Chem Soc 140(15):5037–5040
13. Wang SB, Wang Y, Zhang SL et al (2019) Supporting ultrathin $ZnIn_2S_4$ nanosheets on Co/N-doped graphitic carbon nanocages for efficient photocatalytic H_2 generation. Adv Mater 31(41):1903404
14. Wei YZ, Wan JW, Wang JY et al (2021) Hollow multishelled structured $SrTiO_3$ with La/Rh Co-doping for enhanced photocatalytic water splitting under visible light. Small. https://doi.org/10.1002/smll.202005345
15. Jia TK, Liu M, Zheng CY et al (2020) One pot hydrothermal synthesis of La-doped ZnIn2S4 microspheres with improved visible-light photocatalytic performance. Nanomaterials. 10(10):2026
16. Shi JW, Chen F, Hou LL et al (2021) Eosin Y bidentately bridged on UiO-66-NH_2 by solvothermal treatment towards enhanced visible-light-driven photocatalytic H_2 production. Appl Catal B Environ 280:119385
17. Zhang SY, Du M, Xing ZP et al (2020) Defect-rich and electron-rich mesoporous Ti-MOFs based NH_2-MIL-125(Ti)@$ZnIn_2S_4$/CdS hierarchical tandem heterojunctions with improved charge separation and enhanced solar-driven photocatalytic performance. Appl Catal B: Environ 262:118202
18. He YQ, Rao H, Song KP et al (2019) (2019) 3D hierarchical $ZnIn_2S_4$ nanosheets with rich Zn vacancies boosting photocatalytic CO_2 reduction. Adv Funct Mater 29(45):1905153
19. Wang L, Zhou HH, Zhang HZ et al (2020) Facile in situ formation of a ternary 3D $ZnIn_2S_4$-MoS_2 microsphere/1D CdS nanorod heterostructure for high efficiency visible-light photocatalytic H_2 production. Nanoscale 12(25):13791–13800
20. Cao SY, Wu YZ, Hou JG et al (2020) 3D porous pyramid heterostructure array realizing efficient photo-electrochemical performance. Adv Energy Mater 10(5):1902935
21. Qiu BC, Zhu QH, Du MM et al (2017) Efficient solar light harvesting CdS/Co_9S_8 hollow cubes for Z-scheme photocatalytic water splitting. Angewandte Chemie Int Ed 56(10):2684–2688
22. Zhao XX, Feng JR, Liu J et al (2018) An efficient, visible-light-driven, hydrogen evolution catalyst NiS/$Zn_xCd_{1-x}S$ nanocrystal derived from a metal–organic framework. Angewandte Chemie Int Ed 57(31):9790–9794
23. Zhang TX, Meng FL, Cheng Y et al (2021) Z-scheme transition metal bridge of Co_9S_8/Cd/CdS tubular heterostructure for

enhanced photocatalytic hydrogen evolution. Appl Catal B: Environ 286:119853
24. Zhang J, Yu J, Zhang Y et al (2011) Visible light photocatalytic H_2 production activity of CuS/ZnS porous nanosheets based on photoinduced interfacial charge transfer. Nano Lett 11(11):4774–4779
25. Sheng JL, Chen JH, Kang JH et al (2019) Octahedral Cu_2O@$Co(OH)_2$ nanocages with hierarchical flake-like walls and yolk-shell structures for enhanced electrocatalytic activity. ChemCatChem 11(10):2520–2525
26. Zheng DD, Zhang GG, Wang XC et al (2015) Integrating CdS quantum dots on hollow graphitic carbon nitride nanospheres for hydrogen evolution photocatalysis. Appl Catal B: Environ 179:479–488
27. Ji MW, Li XY, Wang HZ et al (2017) Versatile synthesis of yolk/shell hybrid nanocrystals via ion-exchange reactions for novel metal/semiconductor and semiconductor/semiconductor conformations. Nano Res 10(9):2977–2987
28. Ran L, Yin LW (2017) Double-walled heterostructured $Cu_{2-x}Se$/Cu_7S_4 nanoboxes with enhanced electrocatalytic activity for quantum dot sensitized solar cells. CrystEngComm 19(37):5640–5652
29. Bhavani P, Kumar DP, Shim HS et al (2020) In situ addition of Ni salt onto a skeletal Cu_7S_4 integrated CdS nanorod photocatalyst for efficient production of H_2 under solar light irradiation. Catal Sci Technol 1(11):3542–3551
30. Zhong LX, Mao BD, Liu M et al (2021) Construction of hierarchical photocatalysts by growing $ZnIn_2S_4$ nanosheets on Prussian blue analogue-derived bimetallic sulfides for solar co-production of H_2 and organic chemicals. J Energy Chem 54:386–394
31. Tang R, Yin LW (2015) Enhanced photovoltaic performance of dye-sensitized solar cells based on Sr-doped TiO_2/$SrTiO_3$ nanorod array heterostructures. J Mater Chem A 3(33):17417–17425
32. Xu WW, Tian W, Meng LX et al (2021) Interfacial chemical bond-modulated Z-scheme charge transfer for efficient photoelectrochemical water splitting. Adv Energy Mater 11(8):2003500
33. Tan PF, Zhu AQ, Qiao LL et al (2019) Constructing a direct Z-scheme photocatalytic system based on 2D/2D WO_3/$ZnIn_2S_4$ nanocomposite for efficient hydrogen evolution under visible light. Inorg Chem Front 6(4):929–939
34. Cai XY, Mao L, Yang SQ et al (2018) Ultrafast charge separation for full solar spectrum-activated photocatalytic H_2 generation in a black phosphorus-Au-CdS heterostructure. ACS Energy Lett 3(4):932–939
35. Zhang SQ, Liu X, Liu CB et al (2018) MoS_2 quantum dot growth induced by S vacancies in a $ZnIn_2S_4$ monolayer: atomic-level heterostructure for photocatalytic hydrogen production. ACS Nano 12(1):751–758
36. Swain G, Sultana S, Parida K et al (2019) One-pot-architectured Au- nanodot-promoted MoS_2/$ZnIn_2S_4$: a novel p–n heterojunction photocatalyst for enhanced hydrogen production and phenol degradation. Inorg Chem 58(15):9941–9955
37. Chen YB, Li JF, Liao PY et al (2020) Cascaded electron transition in $CuWO_4$/CdS/CDs heterostructure accelerating charge separation towards enhanced photocatalytic activity. Chin Chem Lett 31(6):1516–1519
38. Xiao R, Zhao CX, Zou ZY et al (2020) In situ fabrication of 1D CdS nanorod/2D Ti_3C_2 MXene nanosheet Schottky heterojunction toward enhanced photocatalytic hydrogen evolution. Appl Catal B: Environ 268:118382
39. Mao L, Cai XY, Zhu MS et al (2021) Hierarchically 1D CdS decorated on 2D perovskite-type $La_2Ti_2O_7$ nanosheet hybrids with enhanced photocatalytic performance. Rare Met 40(5):1067–1076
40. Ding MY, Xiao R, Zhao CX et al (2020) Evidencing interfacial charge transfer in 2D CdS/2D MXene Schottky heterojunctions toward high-efficiency photocatalytic hydrogen production. Sol RRL 5(2):2000414
41. Cai L, Du YC, Guan XJ et al (2019) CdS nanocrystallites sensitized ZnO nanorods with plasmon enhanced photoelectrochemical performance. Chin Chem Lett 30(12):2363–2367
42. Zulfiqar S, Liu S, Rahman N et al (2021) Construction of S-scheme MnO_2@CdS heterojunction with core-shell structure as H_2-production photocatalyst. Rare Met. https://doi.org/10.1007/s12598-020-01616-w

Jungang Hou is a full professor in Dalian University of Technology. He received his PhD degree (2010) from Tianjin University. He joined the Faculty of University of Science and Technology Beijing and was promoted to associate professor in 2013. He worked in Tohoku University as a fellow of Japan Society for the Promotion of Science from 2014 to 2015. His recent research interests focus on the development of photocatalysts and electrocatalysts, photocatalytic and electrocatalytic water splitting, CO_2/N_2 conversion to valuable chemicals, and synthesis and applications of nanostructured materials.

Licheng Sun received his PhD degree in 1990 from Dalian University of Technology. He went to Germany as a postdoc at Max-Planck-Institut für Strahlenchemie with Dr. Helmut Görner (1992–1993) and then as an Alexander von Humboldt fellow at Freie Universität Berlin (1993–1995) with Prof. Harry Kurreck. He moved to the KTH Royal Institute of Technology, Stockholm, in 1995 and became an assistant professor in 1997, an associate professor in 1999 (at Stockholm University), and a full professor in 2004 (KTH). He is now a chair professor and the head of Centers of Artificial Photosynthesis for Solar Fuels at Westlake University. His research interests cover artificial photosynthesis, molecular catalysts for water oxidation and hydrogen generation, functional devices for total water splitting, and solar cells.